Noncontact atomic force microscopy imaging of water dissociation products on TiO_2(110)

C. L. Pang,[1] A. Sasahara,[1,2] H. Onishi,[1] Q. Chen,[3] and G. Thornton[3]
[1]*Department of Chemistry, Faculty of Science, Kobe University, Kobe, 657-8501, Japan*
[2]*Japan Science and Technology Agency, Kawaguchi, Saitama 332-0012, Japan*
[3]*London Centre for Nanotechnology and Chemistry Department, University College London, London WC1H 0AJ, United Kingdom*
(Received 11 July 2006; published 28 August 2006)

We have imaged the products of water dissociation on TiO_2(110) with noncontact atomic force microscopy (NC-AFM). Scanning tunneling microscopy (STM) experiments have revealed that water splits into a hydroxyl group that sits in an O vacancy and an H adatom which lies on a bridging O atom. With this knowledge, STM images acquired in the same area allow an unambiguous identification of these H adatoms in the corresponding NC-AFM images.

DOI: 10.1103/PhysRevB.74.073411 PACS number(s): 68.37.Ps, 68.37.Ef, 68.47.Gh, 68.55.Ln

Titania has been intensively studied since it was discovered that it could photocatalyze the dissociation of water.[1] It is this photocatalytic behavior which underpins the use of titania in applications such as solar cells, water purification, and self-cleaning windows.[2,3] As the most thermodynamically stable face of TiO_2, rutile TiO_2(110) has become the most studied single crystal oxide surface, making it something of a model oxide surface.[4] The TiO_2(110) surface is characterized by alternating rows of fivefold coordinated Ti atoms and bridging-O atoms which run in the [001] direction, as shown in Fig. 1. Ti rows usually appear bright in scanning tunneling microscopy (STM) images whereas the bridging-O rows appear dark, despite the bridging-O rows lying higher in the surface.[4–6] Between the bright Ti rows, point defects appear as bright features (denoted type-*A* defects). These type-*A* defects were assigned first to bridging oxygen vacancies (O vacs) (Ref. 7) then to H adatoms.[8] Subsequently, very high resolution STM images showed that these type-*A* defects can be resolved into two species, one type slightly brighter than the other.[9] The brighter of these two species was attributed to H adatoms, with the darker species assigned to O vacs.[10,11] Water from the residual vacuum was shown to dissociate over the O vacs on TiO_2(110) forming a pair of H adatoms which sit on the bridging-O rows, so that H adatoms are nearly always present on the surface.[10–12] The model in Fig. 1 shows the presence of one O vac and one H adatom.

In this paper, we show for the first time that it is possible to unambiguously identify the products of a surface reaction in noncontact atomic force microscopy (NC-AFM) images. These reaction products are OH groups which result from water dissociation over O vacs on TiO_2(110). To enable the identification of these OH groups, we compare NC-AFM images with STM images of the same area.

The experiments were performed in Kobe using a JSPM-4500A (*JEOL*) microscope operated at room temperature with a base pressure of $\sim 2\times 10^{-10}$ mbar. The rutile TiO_2(110) crystal (*Shinko-sha*) was prepared with cycles of Ar-ion bombardment (2 keV) and annealing to ~1100 K. NC-AFM images were recorded in the constant frequency shift (Δf) mode using conductive silicon cantilevers (*MikroMasch*) with force constants of ~14 Nm^{-1}, resonant frequencies of ~300 kHz, and peak-to-peak amplitudes of ~70 Å. Simultaneous STM images were recorded by measuring the log-current signal during standard Δf-feedback NC-AFM operation with an applied bias of 1.8 V.[13,14] The log-current images are brighter and therefore easier to monitor than linear-current images during data acquisition. These log-current images have been converted into linear current images and are referred to and displayed as such. Since the bandwidth of the tunneling current preamplifier is limited to about 10 kHz, the observed current corresponds to the time-averaged tunneling current ($\bar{I}_t$). Additional STM images were recorded in the constant current mode without oscillation. In all images presented, the sample is biased with the tip held at ground.

Figure 2(a) shows an STM image of the TiO_2(110) surface. Line profiles taken over representative type-*A* defects are shown in Fig. 2(e). These defects resolve into two types, large defects with heights of ~0.8 Å and small defects with heights of ~0.25 Å, similar to previous results.[9–11] To further eliminate the possibility that the large defects on TiO_2(110) have some other origin, we have tested the reactivity of the most prevalent gases in the residual vacuum (water, H_2, CO, and CO_2) and only exposure to water has any effect on STM images at room temperature. In Ref. 11, H-adatom dimers were proposed to coexist with isolated H adatoms with respective heights of ~1.5 Å and ~1 Å. O

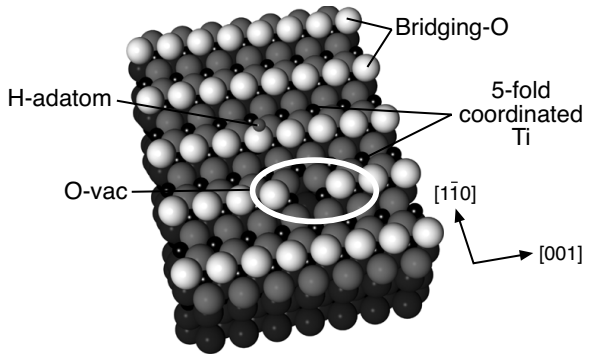

FIG. 1. Ball model of TiO_2(110) including an O vac and an H adatom. Large grey spheres depict lattice oxygen with atoms nearer the surface shaded lighter. Small black spheres indicate Ti atoms. The O vac is circled and the H adatom is represented with a small grey sphere.

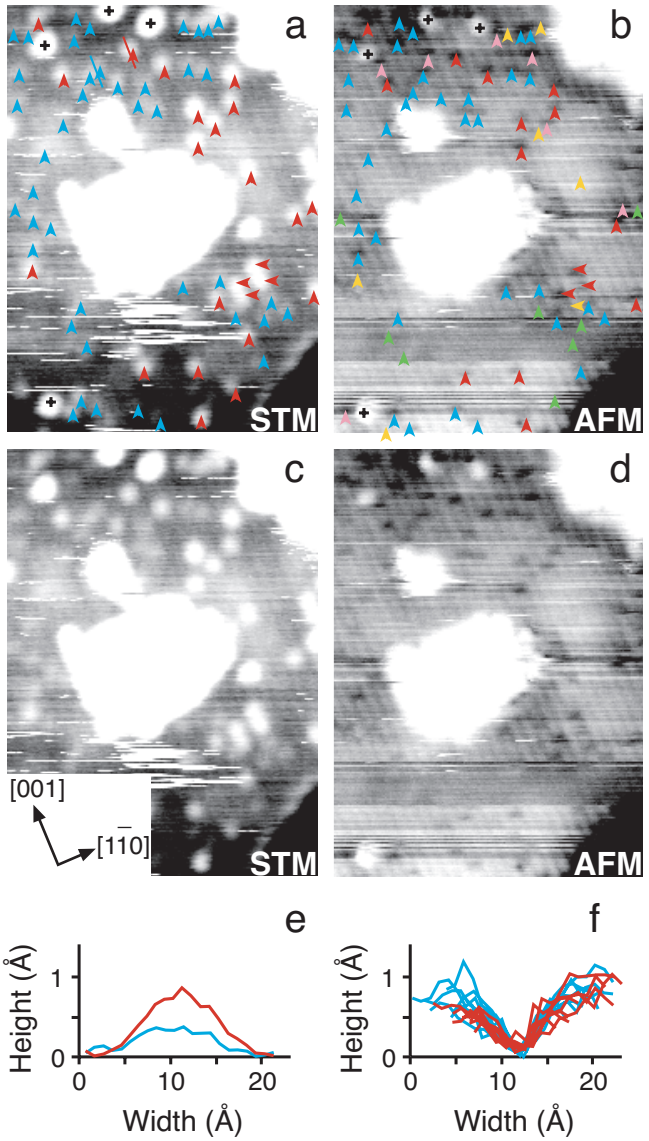

FIG. 2. (Color) 180 Å×250 Å images and line profiles of TiO_2(110). (a) STM image with bias of 1.4 V and tunneling current, 1.0 nA. Blue and red arrowheads indicate O vacs and H adatoms, respectively. Black crosses indicate unknown contaminants. (b) NC-AFM image recorded with $\Delta f = \sim -63$ Hz and applied voltage, 1.4 V. The NC-AFM image was recorded ~3 mins before the STM image in (a). Blue and red arrowheads are marked where depressions correspond to the positions of O vacs and H adatoms in (a), respectively. Green and yellow arrowheads indicate positions where defects are not apparent in (b) but are visible in (a). The green arrowheads clearly lie on areas where the tip is unstable. The defects marked with yellow arrowheads presumably correspond either to defects which cannot be imaged due to a more transient instability or they correspond to defects which have migrated to different positions. Together, the defects which are not imaged clearly in (b) account for ~23% of all the defects in (a). Pink arrowheads indicate defects visible in (b) but not in (a) thereby giving evidence for the migration of defects. For clarity, the images in (a) and (b) are duplicated in (c) and (d), respectively. (e) Representative line profiles taken over an O vac (blue) and an H adatom (red) in the positions indicated by the coloured lines in (a). (f) 16 line profiles taken over depressions in (b) assigned to H adatoms (red) and O vacs (blue).

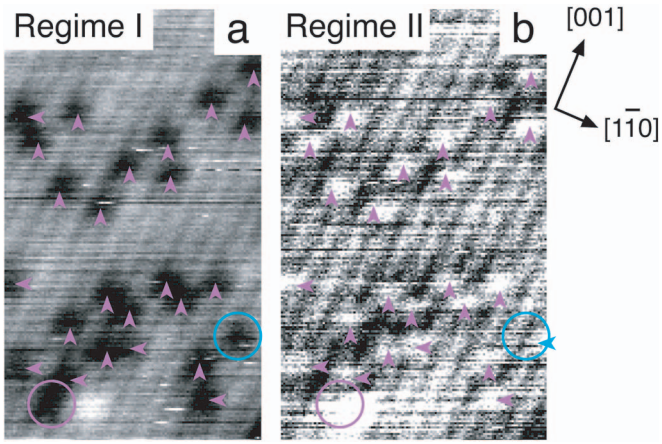

FIG. 3. (Color) 115 Å×185 Å NC-AFM images of TiO_2(110) recorded with $\Delta f = \sim -45$ Hz and applied voltage, 1.4 V. (a) Recorded in *Regime I*. (b) Image recorded in *Regime II* following a tip change between the images. Purple arrowheads indicate coincident type-*A* defects. The blue circle indicates the position of a defect in (a) which appears to have migrated to the right of the frame and is marked with a blue arrow in (b). The purple circle indicates a defect which is observable in (a) but not in (b). We presume this is also due to migration either away from the scan area or onto the tip (Ref. 7). These two defects which are not in the same position as in (a) amount to ~7% of the total number of defects visible.

vacs were found with a height of ~0.5 Å. In the STM image of Fig. 2(a), we find only two defect species, with heights of ~0.8 Å and ~0.25 Å which we therefore assign to isolated H adatoms and O vacs, as indicated with red and blue arrowheads respectively in Fig. 2(a).

The NC-AFM image in Fig. 2(b) is of the same area as the STM image in Fig. 2(a) and was recorded ~3 mins beforehand. Superimposing the same arrowheads from Fig. 2(a) over the NC-AFM image in Fig. 2(b) allows us to identify features in NC-AFM corresponding to both O vacs and H adatoms. Thus, it becomes clear that both O vacs and H adatoms appear as depressions in the bright rows of the NC-AFM image. It is well established that when type-*A* defects are visible in STM, the bright rows correspond to Ti rows.[4,7–11] It therefore follows that the bright rows containing depressions in the NC-AFM image of Fig. 2(b) correspond to bridging-O rows. Figure 2(f) displays NC-AFM line profiles taken along the [001] direction over eight H adatoms and eight O vacs. The profiles have a similar appearance with mean depths of ~0.6±0.2 Å for H adatoms and ~0.5±0.2 Å for O vacs. The FWHM (full-width at half maximum height) widths are ~5.2±1.0 Å for H adatoms and ~5.0±2.3 Å for O vacs, so with the present resolution they are indistinguishable using NC-AFM alone. However, by comparison with the STM image, we can definitively identify the reaction products in the NC-AFM image for the first time. In previous NC-AFM images of TiO_2(110), with the same contrast, such depressions were attributed only to O vacs, based on geometrical considerations.[15] It should be noted that a minority of the type-*A* defects present in the STM image of Fig. 2(a) are not clearly identifiable in the NC-AFM image of Fig. 2(b). This is likely to be due to the greater instability of NC-AFM imaging coupled with some migration of the defects.

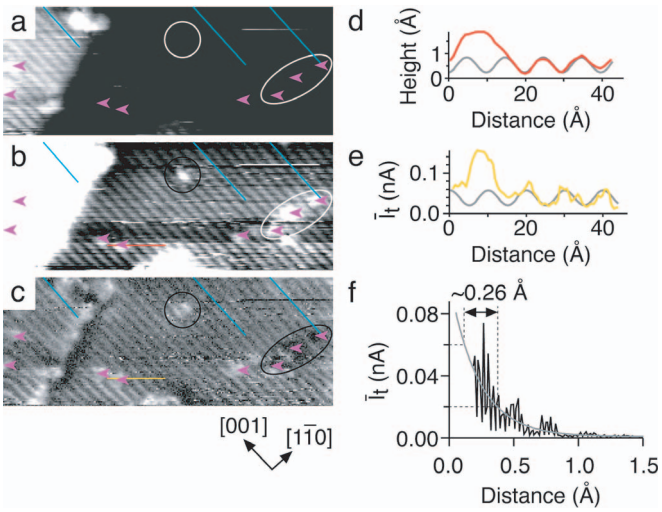

FIG. 4. (Color) (a) 250 Å×90 Å NC-AFM image of TiO_2(110) recorded with $\Delta f = \sim -63$ Hz and applied voltage, 1.8 V. The contrast has been adjusted to highlight the upper terrace. (b) As (a) with the contrast optimized for the lower terrace. (c) Simultaneously recorded $\bar{I}_t$ image. In (a) and (b), type-*A* defects are indicated with purple arrowheads and blue lines are drawn over three bright rows. An identical array of arrowheads and lines are superimposed in the same positions on (c). The blue lines in (c) lie on dark rows and the arrowheads point at type-A defects which appear bright and centred on the bright rows in the $\bar{I}_t$ image. A circle indicates an unidentified impurity in all three images. In all three images, the ellipse indicates three defects which appear dark in the $\bar{I}_t$ image due to the error-contribution. (d) Line profile taken over the red line in (b) showing the position of the defects (between the bright rows) in the topographic image. A sine wave has been fitted to the rows on the right hand side of the graph and is superimposed as a grey curve. (e) Line profile taken over the yellow line in (c) showing the position of the defects (atop the bright rows) in the $\bar{I}_t$-image. A sine wave has been fitted to the rows on the right hand side of the graph and is superimposed as a grey curve. (f) A graph showing calculated $\bar{I}_t$ vs distance. The grey curve is an exponential fit to the data.

Figure 3 shows a pair of NC-AFM images between which a tip change occurs. In the first image shown in Fig. 3(a), type-*A* defects appear as depressions in the bridging-O rows. We define this contrast as *Regime I*. In the second image [Fig. 3(b)], bright features appear between bright rows. These bright features are in the same positions as the depressions in Fig. 3(a) so we can assign the bright features in Fig. 3(b) to type-*A* defects which then indicates that the bright rows are Ti rows. We define the contrast in Fig. 3(b) as *Regime II*. The tip change is probably related to a change in polarity at the tip apex.[16–18] Theoretical simulations of NC-AFM on ionic surfaces have shown that changing the local potential at the tip apex can lead to radically different images. The basic principle is that a tip apex with a negative potential will have a strong attraction to the surface cations which will therefore appear bright in the NC-AFM images. Changing the polarity at the tip apex to a positive potential instead makes the tip apex attracted to the surface anions and they will therefore appear bright in the NC-AFM images. This means that NC-AFM simulations performed on TiO_2(110) with a positive tip apex give bright rows corresponding to the bridging-O rows and those with a negative tip apex show the Ti rows bright.[18]

Figures 4(a) and 4(b) show another NC-AFM image, recorded simultaneously with a time-averaged tunneling current image ($\bar{I}_t$ image), shown in Fig. 4(c). The NC-AFM contrast can be identified as *Regime II* since bright rows are seen with bright type-*A* defects between them, as highlighted in the line profile in Fig. 4(d). The defect density is rather low and may be attributed to tip-induced H desorption due to imaging the same area repeatedly.[7,8,10,11] The expectation is that the $\bar{I}_t$ image will be in phase with the NC-AFM image since STM usually images bright Ti rows. In fact, the $\bar{I}_t$ image is out-of-phase such that the bright rows in STM are in the NC-AFM-indicated positions of bridging-O rows. There are two examples in the literature of bright rows in STM appearing approximately in the positions of the bridging-O rows.[4,7,19] In the first example, these images arise after special pretreatment of a standard tungsten tip consisting of 10 V, 20 nA scans on a Si(100) surface.[19] Such pretreatment is absent in our experiment. In the second example,[4,7] depressions appear on the bright rows and bright spots from type-*A* defects are not visible. In the present case, the line profile in Fig. 4(e) taken from the $\bar{I}_t$ image shows the type-*A* defects as bright spots centred on the bright rows, so we conclude that the $\bar{I}_t$ image is unrelated to either of these special STM conditions.

An additional explanation for the out-of-phase $\bar{I}_t$ image is based on the movement of the tip. In *Regime II*, the tip will move towards the bridging-O rows and away from the Ti rows in order to maintain a constant Δf. This means that there is always an "error contribution" to $\bar{I}_t$ images when Δf is used as the feedback due to the surface topography and this error contribution is always out of phase with the NC-AFM image. The error contribution would not affect the qualitative appearance of TiO_2(110) $\bar{I}_t$ images recorded when the NC-AFM gives bright bridging-O rows such as those that occur in *Regime I*,[13] but could potentially lead to unexpected images in *Regime II*. By analysing $\bar{I}_t$ vs distance curves, we can establish whether the error contribution is large enough to change the qualitative appearance of $\bar{I}_t$ images. However, we were unable to record good quality $\bar{I}_t$ vs distance curves with an oscillating tip. For this reason we employed an alternative approach, which involves recording I_t vs distance curves without oscillation. $\bar{I}_t$ is related to I_t as follows:[14,20]

$$\bar{I}_t = I_t \times \frac{1}{\sqrt{2\pi A/\lambda_T}},$$

where A is the oscillation amplitude and λ_T is the decay length of the tunneling current. This equation only applies, strictly, for harmonic oscillations with $A/\lambda_T \gg 1$, but can be used here because at an amplitude of ~70 Å there should be no significant deviation from harmonic motion and $A/\lambda_T \gg 1$ is satisfied.[14,20] An exponential fit to the data gives $\lambda_T \approx 0.23$ Å, so that $\bar{I}_t \approx I_t/44$. Figure 4(f) shows a graph of the

calculated $\bar{I}_t$ vs distance. The dark rows from the $\bar{I}_t$ image in Fig. 4(c) have $\bar{I}_t$ of ~0.02 nA and the bright rows, ~0.06 nA. The distance in the graph which separates these $\bar{I}_t$ values is ~0.26 Å, which is less than the corrugation (~0.4 Å) of the NC-AFM topography in Figs. 4(a) and 4(b). This supports the possibility that some $\bar{I}_t$ images acquired with Δf feedback can be dominated by the error contribution and this is how we interpret the $\bar{I}_t$ image in Fig. 4(c). The appearance of most of the type-*A* defects as bright features in this $\bar{I}_t$ image shows that they are genuine STM features since the error contribution acts to reduce $\bar{I}_t$, yet $\bar{I}_t$ increases. Notice that for the defects marked with an ellipse, $\bar{I}_t$ has been reduced so much by the error contribution that they appear dark in the $\bar{I}_t$ image. In principle, this error contribution can be removed by recording images in the constant height mode and simultaneously acquiring Δf and $\bar{I}_t$ images. This will be the subject of further work.

Despite some ambiguity in the interpretation of $\bar{I}_t$ images on TiO_2(110) acquired with Δf feedback, such images can still assist in understanding contrast mechanisms in NC-AFM.[18,21] For example, $\bar{I}_t$ images recorded simultaneously with the NC-AFM images in Fig. 3 show that the image in *Regime I* has $\bar{I}_t \approx 0.02$ nA across the bright and dark rows compared with ~0.05 nA in *Regime II*. There could be two explanations for this. All other imaging parameters are identical between the two images. Hence, following the tip change, either the tunneling resistance decreases so that $\bar{I}_t$ increases at the same tip sample separation, or the tip has to move closer to the surface to maintain the same Δf, and $\bar{I}_t$ increases as a consequence. With similar scanning parameters, other images in *Regime I* and *Regime II* have $\bar{I}_t$ values close to 0.02 nA and 0.05 nA, respectively.

In summary, by comparing with STM images recorded in the same area, we have unambiguously identified the products of water dissociation on TiO_2(110) in NC-AFM images. Our work shows that NC-AFM has the potential to follow surface reactions on insulating substrates such as alumina, to which STM cannot be applied. To do so will require that the image contrast of the reaction products is well understood. In principle, this could be achieved by a close comparison with theoretical simulations.

This work was funded by the JSPS (Japan), the CREST of JST (Japan), the EPSRC (U.K.), and the Royal Society (U.K.).

[1] A. Fujishima and K. Honda, Nature (London) **37**, 238 (1972).
[2] B. O'Regan and M. Grätzel, Nature (London) **353**, 737 (1991).
[3] R. Blossey, Nat. Mater. **2**, 301 (2003).
[4] U. Diebold, Surf. Sci. Rep. **48**, 53 (2003).
[5] U. Diebold *et al.*, Phys. Rev. Lett. **77**, 1322 (1996).
[6] H. Onishi, K. Fukui, and Y. Iwasawa, Bull. Chem. Soc. Jpn. **68**, 2447 (1995).
[7] U. Diebold *et al.*, Surf. Sci. **411**, 137 (1998).
[8] S. Suzuki *et al.*, Phys. Rev. Lett. **84**, 2156 (2000).
[9] R. Schaub *et al.*, Phys. Rev. Lett. **87**, 266104 (2001).
[10] O. Bikondoa *et al.*, Nat. Mater. **5**, 189 (2006).
[11] S. Wendt *et al.*, Surf. Sci. **598**, 226 (2005).
[12] I. M. Brookes, C. A. Muryn, and G. Thornton, Phys. Rev. Lett. **87**, 266103 (2001).
[13] M. Ashino *et al.*, Phys. Rev. Lett. **86**, 4334 (2001).
[14] Ch. Loppacher *et al.*, Phys. Rev. B **62**, 16944 (2000).
[15] K. I. Fukui, H. Onishi, and Y. Iwasawa, Phys. Rev. Lett. **79**, 4202 (1997).
[16] C. L. Pang *et al.*, Phys. Rev. B **65**, 201401(R) (2002).
[17] A. S. Foster *et al.*, Phys. Rev. B **66**, 235417 (2002).
[18] A. S. Foster *et al.*, Phys. Rev. B **68**, 195410 (2003).
[19] Q. Guo, I. Cocks, and E. M. Williams, J. Phys. D **31**, 2231 (1998).
[20] F. J. Giessibl and H. Bielefeldt, Phys. Rev. B **61**, 9968 (2000).
[21] Y. Sun *et al.*, Phys. Rev. B **71**, 193407 (2005).